A possible probe to neutron-skin thickness by fragment parallel momentum distribution in projectile fragmentation reactions

Chun-Wang Ma*
College of Physics, Henan Normal University, Xinxiang 453007, China and
Institute of Nuclear Science and Technology, Henan Academy of Sciences, Zhengzhou 450015, China

Yi-Jie Duan, Ya-Fei Guo, Chun-Yuan Qiao, Yu-Ting Wang, Jie Pu, Kai-Xuan Cheng, and Hui-Ling Wei
College of Physics, Henan Normal University, Xinxiang 453007, China

Neutron-skin thickness is a key parameter for a neutron-rich nucleus; however, it is difficult to determine. In the framework of the Lanzhou Quantum Molecular Dynamics (LQMD) model, a possible probe for the neutron-skin thickness (δ_{np}) of neutron-rich ^{48}Ca was studied in the 140A MeV ^{48}Ca + ^{9}Be projectile fragmentation reaction based on the parallel momentum distribution ($p_{//}$) of the residual fragments. A Fermi-type density distribution was employed to initiate the neutron density distributions in the LQMD simulations. A combined Gaussian function with different width parameters for the left side (Γ_L) and the right side (Γ_R) in the distribution was used to describe the $p_{//}$ of the residual fragments. Taking neutron-rich sulfur isotopes as examples, Γ_L shows a sensitive correlation with δ_{np} of ^{48}Ca, and is proposed as a probe for determining the neutron skin thickness of the projectile nucleus.

Keywords: Neutron-skin thickness, Projectile fragmentation, Parallel momentum distribution, Neutron-rich nucleus, Quantum molecular dynamics model

I. INTRODUCTION

The neutron skin thickness, defined as the difference between the root mean square of the neutron and proton density distributions of a nucleus $\delta_{np} \equiv < r_n^2 >^{1/2} - < r_p^2 >^{1/2}$, is an important parameter for neutron-rich nuclei. With the advanced ability of new rare isotope facilities to produce nuclei near proton and neutron drip lines, a new era has commenced for nuclei with exotic structures, particularly for neutron-rich isotopes at extremes [1, 2]. The exact value of δ_{np} is important in research on symmetry energy [3] and neutron stars [4]. It is more important to study δ_{np} of extreme nuclei because they may have a much lower density distribution in the surface region than stable nuclei. Along the history of studying δ_{np} of neutron-rich nuclei, many probes have been proposed based on different theoretical frameworks and via different types of experiments. Projectile fragmentation reactions induced by neutron-proton asymmetric nuclei, as one type of heavy-ion reactions, are typical experimental tools to investigate properties of neutron-rich nuclei, in which the light particle emissions [5, 6], fragment production ratios[7, 8], fragment mass or charge distributions through information entropy analysis [9, 10], etc, are proposed as probes to study the neutron-skin of projectile nuclei to varying degrees of accuracy. Due to the difficulties in measuring neutron density distributions, the neutron-skin thickness of asymmetric nuclei are usually determined in experiments through indirect probes, for example, the giant dipole resonance [11, 12], spin dipole resonance [13], neutron-removal cross section [14], and parity violating electron scattering (for ^{208}Pb [15, 16] and for ^{48}Ca [17]), etc. The momentum distribution of nucleons is widely used to study the structure and properties of atomic nuclei [18–21]. The short-range correlation between nucleons can be experimentally studied by detecting the high-momentum tail of the nucleon momentum distribution using bremsstrahlung γ rays in heavy-ion nuclear reactions [22–24]. The parallel momentum distribution ($p_{//}$) of fragments in breakup or few-body reactions is usually the first evidence of halo or skin nuclei, as in ^{11}Li [18], ^{29}P [25], ^{23}Al [26], ^{31}Ne [27]. Thus, $p_{//}$ of the residual fragments can also be employed to determine δ_{np} within the framework of optical models [28–30]. Experimentally, the $p_{//}$ of fragments is usually used to determine their yields or cross-sections after integration [31], which directly connects the yields of fragments and the nuclear density (and neutron skin thickness) of the projectile nucleus. This makes the $p_{//}$ of fragment in potential be a probe for δ_{np} of projectile nucleus. In this study, $p_{//}$ of the residual fragments in projectile fragmentation reactions was investigated using the Lanzhou quantum molecular dynamics (LQMD) model [32, 33]. It is suggested that the width of $p_{//}$ of the fragment produced in the peripheral collisions is sensitive and could serve as a probe for δ_{np} of the projectile nucleus.

II. MODEL DESCRIPTION

A. The LQMD model

The LQMD model is an isospin- and momentum-dependent transport model that includes all possible elastic and inelastic collision reaction channels during charge

* Corresponding author, machunwang@126.com

exchange. The temporal evolution of nucleons, hyperons, and mesons in a reaction system under a self-consistently generated mean field is governed by Hamilton's equations of motion [32–35]. Based on the Skyrme interactions, isospin-, density-, and momentum-dependent Hamiltonians were constructed [34]. The Hamiltonian of baryons consists of the relativistic energy, effective interaction potential, and momentum-related components.

$$H_B = \sum_i \sqrt{\mathbf{p}_i^2 + m_i^2} + U_{int} + U_{mom}, \tag{1}$$

where $\mathbf{p}_i$ and m_i denote the momentum and mass of the baryons, respectively. U_{int} comprises the Coulomb interaction and the local interaction potential. The local interaction potential is expressed as follows:

$$U_{loc} = \int V_{loc}[\rho(\mathbf{r})] d\mathbf{r}, \tag{2}$$

derived from the Skyrme energy density functional. $V_{loc}(\rho)$ can be written as:

$$\begin{aligned} V_{loc}(\rho) = &\frac{\alpha}{2}\frac{\rho^2}{\rho_0} + \frac{\beta}{1+\gamma}\frac{\rho^{1+\gamma}}{\rho_0^{\gamma}} + E_{sym}^{loc}(\rho)\rho\delta^2 \\ &+ \frac{g_{sur}}{2\rho_0}(\nabla\rho)^2 + \frac{g_{sur}^{iso}}{2\rho_0}[\nabla(\rho_n - \rho_p)]^2, \end{aligned} \tag{3}$$

where ρ_n, ρ_p and $\rho = \rho_n + \rho_p$ are the neutron, proton, and total densities, respectively, and $\delta = (\rho_n - \rho_p)/(\rho_n + \rho_p)$ is isospin asymmetry. The coefficients $\alpha, \beta, \gamma, g_{sur}, g_{sur}^{iso}$, and ρ_0 were set to -215.7 MeV, 142.4 MeV, 1.322, 23 MeV fm^2, -2.7 MeV fm^2, and 0.16 fm^{-3}, respectively. $E_{sym}^{loc}(\rho)$ is the local part of the symmetry energy, which can be adjusted to mimic the predictions of the symmetry energy calculated using microscopic or phenomenological many-body theories.

$$E_{sym}^{loc}(\rho) = \frac{1}{2} C_{sym}(\rho/\rho_0)^{\gamma_s}. \tag{4}$$

The values of C_{sym} and γ_s are 52.5 MeV and 2.0, respectively, which correspond to hard-symmetry energy with a baryon density [34].

U_{mom} takes the form

$$\begin{aligned} U_{mom} = &\frac{1}{2\rho_0}\sum_{i,j,j\neq i}\sum_{\tau,\tau'} C_{\tau,\tau'}\delta_{\tau,\tau_i}\delta_{\tau',\tau_j}\int\int\int d\mathbf{p}d\mathbf{p}'d\mathbf{r} \\ &\times f_i(\mathbf{r},\mathbf{p},t)\ln[\epsilon(\mathbf{p}-\mathbf{p}')^2 + 1]^2 f_i(\mathbf{r},\mathbf{p}',t), \end{aligned} \tag{5}$$

where $C_{\tau,\tau} = C_{mom}(1+x)$, $C_{\tau,\tau'} = C_{mom}(1-x)$ $(\tau \neq \tau')$ and the isospin symbols $\tau(\tau')$ represent protons and neutrons, respectively. The parameters C_{mom} and ϵ were determined by fitting the real part of the optical potential as a function of the incident energy from the proton-nucleus elastic scattering data, and the obtained values of C_{mom} and ϵ were 1.76 MeV and 500 c^2/GeV^2, respectively. Thus, the effective mass of the nuclear medium at saturation density is m^*/m=0.75. The parameter x is the strength of the isospin splitting, for which a value of -0.65 is adopted in this study, and the mass splitting is $m_n^* > m_p^*$ in the nuclear medium [36].

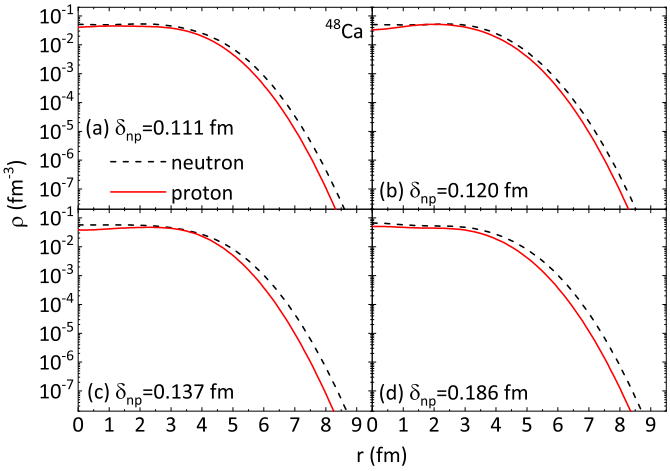

FIG. 1. (Color online) The proton and neutron physical density distributions in the initialization of ^{48}Ca in the LQMD simulation with different δ_{np}. In panels (a), (b), (c), and (d), δ_{np} are 0.111, 0.120, 0.137, and 0.186 fm, respectively.

During the initialization of the projectile nucleus in LQMD, the initial coordinates of the nucleons are obtained by random sampling according to the two-parameter Fermi-type density distribution [38]:

$$\rho_i(r) = \frac{\rho_i^0}{1 + \exp\left(\frac{r - C_i}{f_i t_i / 4.4}\right)}, i = n, p, \tag{6}$$

where ρ_i^0 is a normalization constant that ensures that the integrated density distribution is equal to the number of protons or neutrons, f_i is a parameter for adjusting the diffuseness parameter [7, 39], t_i is the diffuseness parameter, C_i is the half-density radius. Nuclei with reliable stability and an expected neutron skin thickness were selected as candidates for collisions, and the values of δ_{np} were 0.111, 0.120, 0.136, 0.168, and 0.186 fm for the corresponding initial ^{48}Ca nuclei after LQMD initialization (see Fig. 1). The fragments were analyzed in phase space at t = 300 fm/c in the LQMD simulation, and nucleons with a relative distance smaller than 3.0 fm and a relative momentum smaller than 200 MeV/c were considered in the coalescence model [33].

B. Parallel momentum distribution

The $p_{//}$ of the fragments produced in projectile fragmentation reactions exhibits a nonsymmetric distribution in experiments, which can be fitted by a combined

Gaussian function [31],

$$\frac{d\Gamma}{dp} = \begin{cases} S \times \exp\left(-\frac{(p-p_0)^2}{2\Gamma_L^2}\right), & \text{if } p \le p_0, \\ S \times \exp\left(-\frac{(p-p_0)^2}{2\Gamma_R^2}\right), & \text{if } p > p_0. \end{cases} \quad (7)$$

In the combined Gaussian function, the left and right halves have the same peak position, but different widths. S is the normalization factor, p_0 is the peak position of the distribution, Γ_L and Γ_R denote the widths of the left and right sides of the combined Gaussian distribution, respectively.

III. RESULTS AND DISCUSSION

$p_{//}$ of a fragment is generally influenced by the incident energy of the reaction, nuclear density of the reaction system, impact parameter, and the fragment itself (such as isospin). The experimental δ_{np} determined from the proton elastic scattering for ^{40}Ca was $-0.010^{+0.022}_{-0.024}$ fm [37], and for ^{48}Ca, it was $0.121\pm0.026(exp)\pm0.024(model)$ fm from the parity-violating method [17]. To compare the sensitivity of $p_{//}$ to the projectile nuclear density distribution, the ^{33}P produced in the 140A MeV ^{40}Ca + ^{9}Be ($\delta_{np} = -0.030$ fm of ^{40}Ca) and ^{48}Ca + ^{9}Be ($\delta_{np} = 0.168$ fm of ^{48}Ca) reactions are simulated and fitted by Eq. (7), as shown in Fig. 2. $p_{//}$ for ^{33}P in the symmetric ^{40} Ca-induced reaction is also symmetric in Γ_L and Γ_R, whereas Γ_L is larger than Γ_R for ^{33}P in the asymmetric ^{48} Ca-induced reaction, indicating a neutron-skin effect for the neutron-rich projectile.

With the varying impact parameters in projectile fragmentation reactions, the $p_{//}$ of a specific fragment is also influenced by the significant change in nuclear density from central to peripheral collisions [23], and the $p_{//}$ of a fragment thus carries significant information on reactions, such as nuclear density distribution and nucleon-nucleon cross section [1]. The $p_{//}$ values of the neutron-proton symmetric fragment ^{24}Mg produced in the 140A MeV ^{48}Ca + ^{9}Be reaction within b = [0-2], [2-4], [4-6], and [6-8] fm are plotted in Fig. 3. From the central to the peripheral collisions, $p_{//}$ for ^{24}Mg shifts from the low-momentum side to the high-momentum side as b increases. Both Γ_L and Γ_R depend on impact parameters. For different $p_{//}$, the value of Γ_L tends to decrease with an increase in b. $\Gamma_L > \Gamma_R$ (Fig. 3), with the uncertainty of the Γ_R larger than that of Γ_L, (particularly for the central collisions). Γ_R remains constant when $b < 6$ fm whereas Γ_L decreases with increasing b. The reason for $\Gamma_L > \Gamma_R$ may be the difference in the centrality in the reaction; that is, the larger the centrality, the deeper the collision with the target, and the significant $p_{//}$ lost, as well as the wider width of Γ_L.

Finally, the $p_{//}$ values for the isotopic fragments with different isospins were studied to determine whether they are sensitive to the neutron skin thickness of the projectile. The neutron skin of the asymmetric nucleus mainly

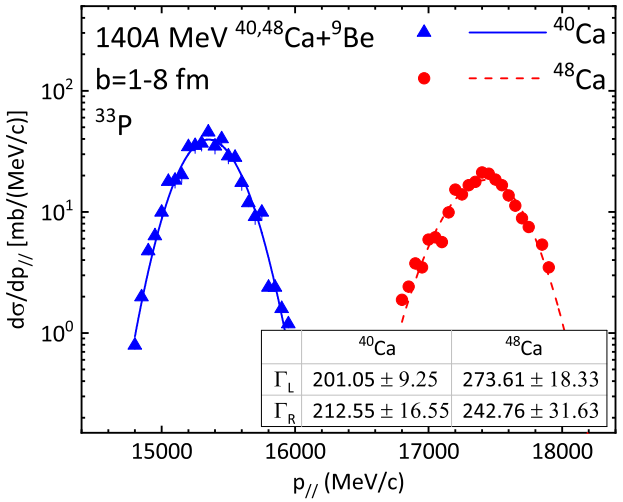

FIG. 2. (Color online) The $p_{//}$ of ^{33}P fragments produced in the LQMD model simulated 140A MeV ^{40,48}Ca + ^{9}Be reactions within b = [1-8] fm. The circles and triangles denote results for the ^{33}P fragments in the ^{48}Ca ($\delta_{np} = 0.168$ fm) and ^{40}Ca ($\delta_{np} = -0.030$ fm) induced reactions, respectively. The lines with different types denote the fitting results by a function according to Eq. (7).

influences the products of peripheral collisions. The $p_{//}$ of the fragments was simulated for peripheral collisions of 140A MeV ^{48}Ca + ^{9}Be within b = [6-8] fm. To compare $p_{//}$ values for isotopic fragments with different mass numbers, $p_{//}$ per nucleon ($p_{//}/A$) was chosen. Based on the different values of δ_{np} for ^{48}Ca, as shown in Fig. 1, the $p_{//}/A$ distributions for neutron-rich sulfur isotopes (from ^{33}S to ^{36}S) are plotted in Fig. 4 together with the fitting results by Eq. (7). The values of Γ_L for $p_{//}$ were obtained and the Γ_L correlations for the sulfur isotopes with δ_{np} of ^{48}Ca are plotted in Fig. 5, in which the correlations are fitted using the decaying exponential function. A strong exponential dependence of Γ_L for neutron-rich sulfur isotopes on δ_{np} of the projectile nucleus ^{48}Ca is shown, which indicates that Γ_L can be an effective probe for the neutron skin thickness of the projectile nucleus in the projectile fragmentation reaction. Further simulations of the fragment de-excitation were performed using the GEMINI code [40]. Compared with the obvious correlation between Γ_L and δ_{np} in the LQMD simulations, Γ_L becomes constant as δ_{np} varies in the LQMD + GEMINI simulations, indicating that the GEMINI de-excitation erases the correlation between Γ_L and δ_{np}. It is also noted that the correlation between Γ_L and δ_{np} is an indirect probe for the neutron-skin thickness of the projectile nucleus because fragments are obtained after the compression-expansion process of the colliding system. Further investigations are also needed to study the $\Gamma_L \sim \delta_{np}$ correlation, including the de-excitation effects, since they may modify the intermediate mass fragments in projectile fragmentation reactions, as has been found

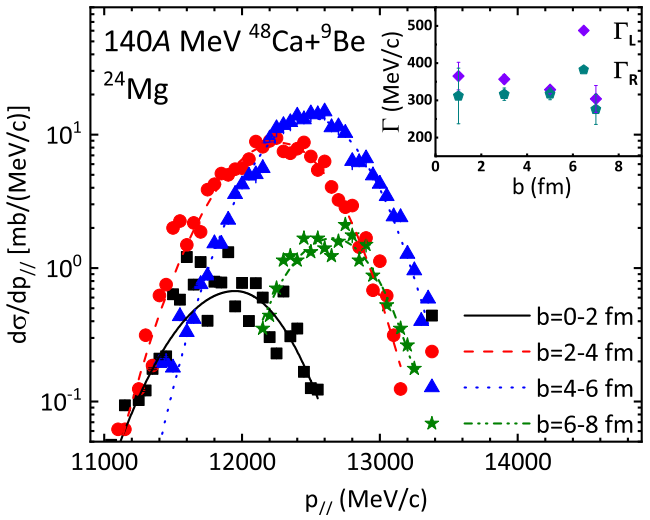

FIG. 3. (Color online) The $p_{//}$ for ^{24}Mg produced in the 140A MeV ^{48}Ca + ^{9}Be (δ_{np} = 0.111 fm of ^{48}Ca) projectile fragmentation reactions at different ranges of impact parameter from central collisions to peripheral collisions. The ranges of b are within [0-2], [2-4], [4-6], and [6-8] fm, respectively. The lines of different types denote the fitting results by a function according to Eq. (7). The inserted figure are for Γ_L and Γ_R for the $p_{//}$.

in Refs. [7, 8].

Based on the eikonal distorted-wave impulse approximation (DWIA) explanation by Ogata et al. [30], the high-momentum side reflects the phase-volume effect owing to energy and momentum conservation, whereas the low-momentum side reflects the momentum shift caused by the attractive potential of the residual nucleus when the incident energy is not very high (below 200A MeV). Because the impact parameters are restricted to b = [6-8] fm, the width of Γ_L reflects the Heisenberg uncertainty principle in quantum mechanism; that is, from $\Delta x \cdot \Delta p \geq \frac{h}{4\pi}$, Δx is inversely correlated to Δp [21]. Thus, it can be considered that the larger the Γ_L, the closer the nucleons contained in the fragment are to the center of the nucleus. In contrast, the smaller the Γ_L, the closer the nucleons in the fragment to the edge of the nucleus. With an increased neutron-skin thickness, the valence neutrons are further pushed away from the center of the nucleus, resulting in a narrower Γ_L as observed in Fig. 4 for the neutron-rich sulfur fragments.

IV. SUMMARY

In summary, a possible probe for the neutron skin thickness of a neutron-rich projectile nucleus was studied by simulating the 140A MeV ^{48}Ca + ^{9}Be reaction in the framework of the LQMD model. The neutron skin thickness of ^{48}Ca was adjusted by varying the diffuseness of the neutron density distributions. A combined Gaussian function with different widths of the left (Γ_L) and right (Γ_R) halves was employed to fit $p_{//}$ of the fragments. The $p_{//}$ values of the fragments are influenced by the projectile nucleus, impact parameters, and the isospin of isotope. It was found that Γ_L of the $p_{//}$ of the projectile-like fragments produced in peripheral collisions was sensitive to δ_{np} of the projectile nucleus. Considering that $p_{//}$ of fragments is easy to measure in experiments, the correlation between Γ_L of the projectile-like fragments and δ_{np} of the projectile nucleus potentially provides a new probe for the neutron skin thickness of neutron-rich projectile nuclei.

ACKNOWLEDGEMENTS

This work is supported by the National Natural Science Foundation of China (Grant Nos. 12375123, 11975091 and 12305130), Natural Science Foundation of Henan Province (Grant No. 242300421048), China Postdoctoral Science Foundation (Grant No. 2023M731016), and Henan Postdoctoral Foundation (Grant No. HN2022164). Ma and Duan thank Prof. Junlong Tian in Guangxi Normal University for useful discussion in manuscript preparation and its revision.

[1] C. W. Ma, H. L. Wei, X. Q. Liu *et al.*, Nuclear fragments in projectile fragmentation reactions, Prog. Part. Nucl. Phys. **121**, 103911 (2021). DOI:10.1016/j.ppnp.2021.103911

[2] X. B. Wei, H. L. Wei, Y. T. Wang *et al.*, Multiple-models predictions for drip line nuclides in projectile fragmentation of ^{40,48}Ca, ^{58,64}Ni, and ^{78,86}Kr at 140 MeV/u, Nucl. Sci. Tech. **33**, 155 (2022). DOI:10.1007/s41365-022-01137-4

[3] L. Li, F. Y. Wang, Y. X. Zhang, Isospin effects on intermediate mass fragments at intermediate energy-heavy ion collisions, Nucl. Sci. Tech. **33**, 58 (2022). DOI:10.1007/s41365-022-01050-w

[4] W. J. Xie, Z. W. Ma, J. H. Guo, Bayesian inference of the crust-core transition density via the neutron-star radius and neutron-skin thickness data, Nucl. Sci. Tech. **34**, 91 (2023). DOI:10.1007/s41365-023-01239-7

[5] X. Y. Sun, D. Q. Fang, Y. G. Ma *et al.*, Neutron/proton ratio of nucleon emissions as a probe of neutron skin, Phys. Lett. B **682**, 396 (2010). DOI:10.1016/j.physletb.2009.11.031

[6] D. Q. Fang, Neutron skin thickness and its effects in nuclear reactions, Nucl. Tech. **46**, 155 (2023). (In Chinese) DOI: 10.11889/j.0253-3219.2023.hjs.46.080016

[7] Z. T. Dai, D. G. Fang, Y. G. Ma *et al.*, Triton/^{3}He ratio as an observable for neutron-skin thickness, Phys. Rev. C **89**, 014613 (2014). DOI:10.1103/PhysRevC.89.014613

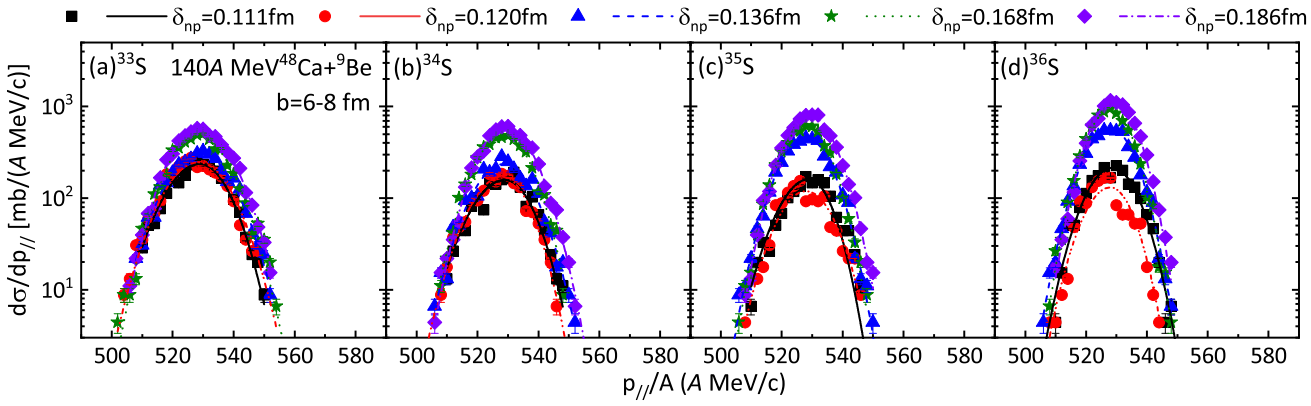

FIG. 4. (Color online) The LQMD simulated $p_{//}/A$ in peripheral collisions (within b = [6-8] fm) for the 140A MeV ^{48}Ca + ^{9}Be reaction. The values of δ_{np} for ^{48}Ca are 0.111, 0.120, 0.136, 0.168, and 0.186 fm, respectively. Panel (a) is for ^{33}S, (b) for ^{34}S, (c) for ^{35}S, and (d) for ^{36}S. The lines denote the fitting results by Eq. (7).

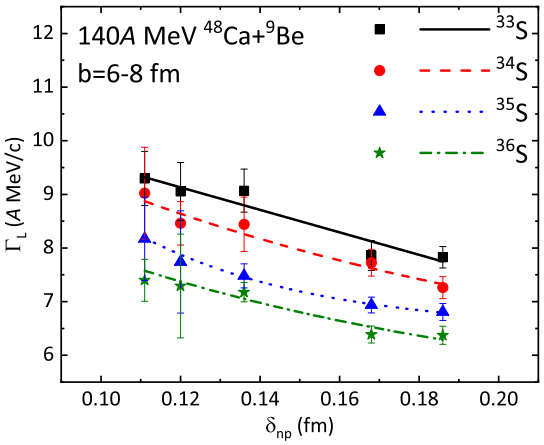

FIG. 5. (Color online) The correlation between Γ_L of $p_{//}$ for neutron-rich sulfur fragments in Fig. 4 and δ_{np} of ^{48}Ca in the LQMD simulated peripheral collisions for 140A MeV ^{48}Ca + ^{9}Be reactions within b = [6-8] fm. The lines of different types denote the exponential fits to the correlations for $^{33-36}$S.

[8] Z. T. Dai, D. Q. Fang, Y. G. Ma *et al.*, Effect of neutron skin thickness on projectile fragmentation, Phys. Rev. C **91**, 034618 (2015). DOI:10.1103/PhysRevC.91.034618

[9] C. W. Ma, Y. P. Liu, H. L. Wei *et al.*, Determination of neutron-skin thickness using configurational information entropy, Nucl. Sci. Tech. **33**, 6 (2022). DOI:10.1007/s41365-022-00997-0

[10] H. L. Wei, X. Zhu, C. Yuan, Configurational information entropy analysis of fragment mass cross distributions to determine the neutron skin thickness of projectile nuclei, Nucl. Sci. Tech. **33**, 111 (2022). DOI:10.1007/s41365-022-01096-w

[11] A. Krasznahorkay, J. Bacelar, J. A. Bordewijk *et al.*, Excitation of the isovector giant dipole resonance by inelastic α scattering and the neutron skin of nuclei, Phys. Rev. Lett. **66**, 1287 (1991). DOI:10.1103/PhysRevLett.66.1287

[12] M. Csatlós, A. Krasznahorkay, D. Sohler *et al.*, Measurement of neutron-skin thickness in ^{208}Pb by excitation of the GDR via inelastic α-scattering, Nucl. Phys. A **719**, 304c (2003). DOI:10.1016/S0375-9474(03)00937-0

[13] C. Gaarde, J. Rapaport, T. N. Taddeucci *et al.*, Excitation of giant spin-isospin multipole vibrations, Nucl. Phys. A **369**, 258 (1981). DOI:10.1016/0375-9474(81)90019-1

[14] D. Q. Fang, Y. G. Ma, X. Z. Cai *et al.*, Effects of neutron skin thickness in peripheral nuclear reactions, Chin. Phys. Lett. **28**, 102102 (2011). DOI:10.1088/0256-307X/28/10/102102

[15] S. Abrahamyan, Z. Ahmed, H. Albataineh *et al.*, Measurement of the neutron radius of ^{208}Pb through parity violation in electron scattering, Phys. Rev. Lett. **108**, 112502 (2012). DOI:10.1103/PhysRevLett.108.112502

[16] D. Adhikari, H. Albataineh, D. Androic *et al.* (PREX Collaboration), Accurate determination of the neutron skin thickness of ^{208}Pb through parity-violation in electron scattering, Phys. Rev. Lett. **126**, 172502 (2021). DOI:10.1103/PhysRevLett.126.172502

[17] D. Adhikari, H. Albataineh, D. Androic *et al.* (CREX Collaboration), Precision Determination of the Neutral Weak Form Factor of ^{48}Ca, Phys. Rev. Lett., **129**, 042501 (2022). DOI:10.1103/PhysRevLett.129.042501

[18] I. Tanihate, H. Hamagaki, O. Hashimoto *et al.*, Measurements of interaction cross sections and nuclear radii in the light p-shell region, Phys. Rev. Lett. **55**, 2676 (1985). DOI:10.1103/PhysRevLett.55.2676

[19] E. Hanelt, A. Grewe, K. H. Schmidt *et al.*, Momentum distributions of projectile fragments produced in the cold and hot fragmentation of relativistic ^{136}Xe and ^{197}Au projectiles, Z. Phys. A **346**, 43 (1993). DOI:10.1007/BF01290780

[20] Y. G. Ma, R. Wada, K. Hagel *et al.*, Sequential decay distortion of Goldhaber model widths for spectator fragments, Phys. Rev. C **65**, 051602 (2002). DOI:10.1103/PhysRevC.65.051602

[21] M. Q. Ding, D. Q. Fang, Y. G. Ma, Effects of neutron-skin thickness on light-particle production, Phys. Rev. C **109**, 024616 (2024). DOI:10.1103/PhysRevC.109.024616

[22] O. Hen, G. A. Miller, E. Piasetzky *et al.*, Nucleon-nucleon correlations, short-lived excitations, and the quarks within, Rev. Mod. Phys. **89**, 045002 (2017). DOI:10.1103/RevModPhys.89.045002

[23] Y. H. Qin, Q. L. Niu, D. Guo *et al.*, Probing high-momentum component in nucleon momentum distribution by neutron-proton bremsstrahlung γ-rays in heavy ion reactions, Phys. Lett. B **850**, 138514 (2024). DOI:10.1016/j.physletb.2024.138514

[24] D. W. Si, Y. Zhou, S. Xiao *et al.*, Measurement of the high energy γ-rays from heavy ion reactions using Čerenkov detector, Nucl. Sci. Tech. **35**, 24 (2024). DOI:10.1007/s41365-024-01368-7

[25] Y. B. Wei, Y. G. Ma, X. Z. Cai *et al.*, Parallel momentum distribution of ^{28}Si Fragments from ^{29}P, Chin. Phys. Lett. **22**, 61 (2005). http://iopscience.iop.org/0256-307X/22/1/018

[26] D. Q. Fang, W. Guo, C. W. Ma *et al.*, Studies on the exotic structure of ^{23}Al, Chin. Phys. C **32**, 34 (2008). http://csnsdoc.ihep.ac.cn/article/id/68c4071e-1596-4366-8926-9446db4e3d07

[27] S. Y. Zhang, S. S. Zhang, X. X. Sun *et al.*, Study of the deformed halo nucleus ^{31}Ne with Glauber model based on microscopic self-consistent structures, Sci. China: Phys. Mech. Astron. **65**, 262011 (2022). DOI:10.1007/s11433-022-1894-6

[28] B. Abu-Ibrahim, Y. Ogawa, Y. Suzuki *et al.*, Cross section calculations in Glauber model: I. Core plus one-nucleon case, Comp. Phys. Commun. **151**, 369 (2003). DOI:10.1016/S0010-4655(02)00734-8

[29] K. Hencken, G. Bertsch, H. Esbensen, Breakup reactions of the halo nuclei ^{11}Be and ^{8}B, Phys. Rev. C **54**, 3043 (1996). DOI:10.1103/PhysRevC.54.3043

[30] K. Ogata, K, Yoshida, K. Minomo, Asymmetry of the parallel momentum distribution of (p, pN) reaction residues, Phys. Rev. C **92**, 034616 (2015). DOI:10.1103/PhysRevC.92.034616

[31] M. Mocko, M. Andronenko, F. Delaunay *et al.*, Projectile fragmentation of ^{40}Ca, ^{48}Ca, ^{58}Ni, and ^{64}Ni at 140 MeV/nucleon, Phys. Rev. C **74**, 054612 (2006). DOI:10.1103/PhysRevC.74.054612

[32] Z. Q. Feng, Momentum dependence of the symmetry potential and its influence on nuclear reactions, Phys. Rev. C **84**, 024610 (2011). DOI:10.1103/PhysRevC.84.024610

[33] Z. Q. Feng, Effects of isospin dynamics on neck fragmentation in isotopic nuclear reactions, Phys. Rev. C **94**, 014609 (2016). DOI:10.1103/PhysRevC.94.014609

[34] Z. Q. Feng, Nuclear in-medium effects and collective flows in heavy-ion collisions at intermediate energies, Phys. Rev. C **85**, 014604 (2012). DOI:10.1103/PhysRevC.85.014604

[35] Y. F. Guo, P. H. Chen, F. Niu *et al.*, Isospin effect in peripheral heavy-ion collisions at Fermi energies, Chin. Phys. C **42**, 124106 (2018). DOI:10.1088/1674-1137/42/12/124106

[36] Z. Q. Feng, Nuclear in-medium and isospin effects on subthreshold kaon production in heavy-ion collisions, Phys. Rev. C **87**, 064605 (2013). DOI:10.1103/PhysRevC.87.064605

[37] J. Zenihiro, H. Sakaguchi, S. Terashima *et al.*, Direct determination of the neutron skin thicknesses in ^{40,48}Ca from proton elastic scattering at $E_p = 295$ MeV, arXiv: 1810. 11796 (2018). DOI:10.48550/arXiv.1810.11796

[38] W. D. Myers, K. H. Schmidt, An update on droplet-model charge distributions, Nucl. Phys. A **410**, 61 (1983). DOI:10.1016/0375-9474(83)90401-3

[39] C. W. Ma, Y. Fu, D. Q. Fang *et al.*, A possible experimental observable for the determination of neutron skin thickness, Chin. Phys. B **17**, 1216 (2008). DOI:10.1088/1674-1056/17/4/011

[40] R. J. Charity, M. A. McManhan, G. J. Wozniak *et al.*, Systematics of complex fragment emission in niobium-induced reactions, Nucl. Phys. A **483**, 371 (1988). DOI:10.1016/0375-9474(88)90542-8